Submitted to Journal of Membrane Science, September 2017

EFFECT OF DIFFERENT AQUEOUS SOLUTIONS OF PURE SALTS AND SALT MIXTURES IN CLOSED-LOOP REVERSE ELECTRODIALYSIS SYSTEMS

M. Micari[a], M. Bevacqua[a], A. Cipollina[a], A. Tamburini[a*], W. Van Baak[b], T. Putts[b], G. Micale[a]

[a] *Dipartimento dell'Innovazione Industriale e Digitale (DIID) - Ingegneria Chimica, Gestionale, Informatica, Meccanica, Università di Palermo (UNIPA) – viale delle Scienze Ed.6, 90128 Palermo, Italy.*

[b] *FUJIFILM Manufacturing Europe BV, Oudenstaart 1, P.O. Box 90156, 5000LJ, Tilburg, The Netherlands.*

[*]*Corresponding author: alessandro.tamburini@unipa.it*

Abstract

Reverse Electrodialysis in a closed-loop arrangement is a viable way to convert low-grade heat into electric power. For the first time, the present work experimentally investigates the use of pure salt-water and equimolar two salts-water as feed solutions in a lab-scale RED unit in terms of *OCV*, stack resistance and corrected power density. The pure salts and the mixture salts to be employed were chosen via a computational analysis. Effect of feed solution velocity and concentration was also investigated. Results concerning the pure salt-water experiments suggest the use of NH_4Cl in the concentration range investigated, while higher power density values are expected with the use of LiCl at larger concentrations. As regards the salt binary mixtures, in some cases the measured stack electrical resistance was found lower than both the two values measured for the corresponding pure salts, thus resulting into higher power density values for the mixtures. This surprising experimental evidence suggests that it is possible to increase the power produced by a conventional RED unit by adding an equivalent molar quantity of another suitable salt. Finally, among the mixtures tested, the NH_4Cl-LiCl mixture appears as the most promising, thanks to the combination of the favorable properties of these two salts.

Keywords:

Reverse Electrodialysis Heat Engine; Closed loop RED; Salt mixture; Salinity Gradient Power

1. INTRODUCTION

The continuous growth of the energy demand is giving impulse to the search and the development of new renewable energy sources. Among these, the energy deriving from salinity gradients (i.e. Salinity Gradient Power, SGP) represents a promising option [1]. This form of energy is available whenever two solutions at different concentration are put in contact and is progressively dissipated while the two solutions are naturally mixing together. Performing a "*controlled mixing*" between the two solutions to convert the chemical potential difference into available power is the goal of all the SGP technologies [2]. Among these, Pressure Retarded Osmosis (PRO) and Reverse Electrodialysis (RED) have reached the highest technology readiness level and currently are the most investigated [3].

Pressure Retarded Osmosis is based on the use of osmotic membranes to convert the salinity gradient energy into mechanical power [4–6], while Reverse Electrodialysis makes use of ionic exchange membranes (IEMs) to allow a direct conversion into electric power.

The properties of IEMs represent one of the most crucial aspects affecting the performance of a RED unit [7]: the perm-selectivity (i.e. transport selective properties) of an IEM towards its counter-ion dramatically affects the process driving force [8], while the IEM electrical resistance may significantly reduce the producible power [9] as it often represents the highest contribution to the stack resistance [10].

RED has been traditionally studied as a viable way to exploit either naturally existing salinity gradients as river estuaries [11] or artificial gradients based on the use of industrial brines as those deriving from desalination plants [12] or saltworks [13]. In both cases, almost all studies have focused on the use of aqueous solutions with sodium-chloride as the main (or only) solute. With this regard, IEMs have been progressively studied and developed in order to enhance their performance and capability to efficiently deal with this kind of solutions.

As an alternative to its traditional application, very recently, RED has been studied as a viable way to convert low-grade waste heat into electrical power by taking advantage from a closed-loop configuration [1,14]. The RED Heat Engine (REDHE) [15,16] is mainly composed of a RED unit and of a regeneration unit: the RED unit is devoted to converting the salinity gradient into electric power by mixing the two solutions at

different concentration, while the regeneration unit makes use of unworthy thermal power to separate them and restore the initial salinity gradient. Note that the economic feasibility of the process is closely related to the use of a cheap thermal source as it occurs for industrial heat at temperatures below 100°C commonly considered as useless or even as a disposal cost (e.g. cooling tower). Of course, solar and geothermal heat may represent valid alternatives.

According to the regeneration step, two different regeneration strategies have been presented for the REDHE: the "solvent extraction" scheme, and the "salt extraction" scheme [15], which are depicted in Figure 1. In the first case, the restore of the initial salinity gradient is based on the use of a regeneration unit which recovers the solvent from the concentrate solution: to this purpose any thermal (e.g. Multi Effect Distillation [17]) or hybrid membrane-thermal desalination technology (as Membrane Distillation [18]) could be a viable possibility. Conversely, in the salt extraction scheme, the restore is guaranteed by the recovery from the dilute solution of the electrolyte transferred within the RED unit [19,20].

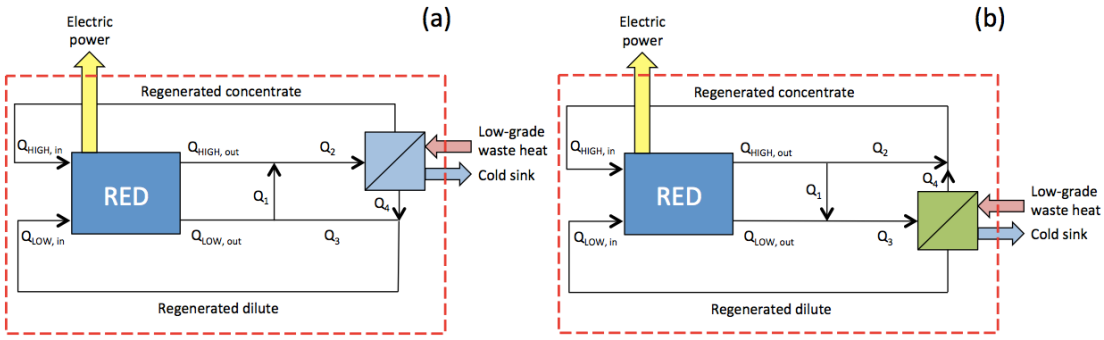

Figure 1: Reverse Electrodialysis Heat Engine regeneration strategies: the solvent extraction scheme on the left (a) and the sat extraction scheme on the right (b) [15].

Within the above closed-loop arrangement the geographical need for estuaries or for industries producing brines along with pre-treatments are no long a limitation, thus guaranteeing a really higher versatility and flexibility to the RED process. More important, this framework also allows the use of artificial solutions composed of any solvent-solute couple with the aim of maximizing the process output (i.e. the cycle efficiency): for instance, salts different than NaCl or mixtures of two or more salts may be used to generate and exploit a higher theoretical potential difference. Moreover, operating conditions in terms of solutions concentration and velocity are no more dependent on the available stream but can be easily tuned to maximize the REDHE

performance. With this regard, the investigation of RED units fed by non conventional (i.e. NaCl-water) solutions is nowadays a topic of crucial importance.

Surprisingly, only a very few studies have been presented so far on the use of a RED unit fed with salts different from NaCl. Some of them regard the investigation of the performance of multivalent ions in a RED unit, mainly referring to the most common ions present in seawater (Mg^{2+}, Ca^{2+} and SO_4^{2-}) in order to predict the behaviour of a RED stack fed by natural seawater [21–23]. Other studies concern the use of thermolytic salts, such as ammonium hydrogen carbonate (NH_4HCO_3). These salts are able to decompose into ammonia, carbon dioxide and water at temperatures of about 40-45°C. Thus, they can be used within a salt extraction regeneration strategy [20,24,25] in a REDHE. Unfortunately, power densities lower than those obtainable with NaCl solutions have been reported [19,24] so far. Other studies focus on the interaction between specific ions and IEMs without investigating the RED process performance: in particular these studies investigate how membrane properties, such as electrical resistance and permselectivity, can be affected by a specific ion [8,26]. For instance, Cassady et al. [26] demonstrated how the permselectivity is not only influenced by the membrane water content, but also by the strength of the ionic interaction between counter-ion and fixed charge groups. Choi et al. [27] studied the effect of various electrolytes on the transport phenomena across the ionic exchange membranes. Martí-Calatayud et al. [28] investigated the possibility of treating industrial waste-water effluents containing metals via electrodialysis: they showed how the membrane structure and the ions size may influence the competitive ion transport. Other studies deal with the determination of the diffusion coefficient of some counter- and co-ions, in order to understand the transport mechanism through IEMs and to model their internal structure [29].

Summarizing, an insufficient amount of data has been collected so far on the performances of a RED unit fed by non-conventional salt-water solutions including pure and mixture salts. Therefore, the present work aims at filling this gap in the literature by selecting the most promising salts to be fed in a RED unit either as pure salt or together as couple (i.e. binary mixture) and at experimentally measuring the main parameters of a RED unit (fed by these non-conventional solutions) including OCV, stack resistance and power density.

2. PURE AND MIXTURE SALTS SELECTION

2.1 Pure salts selection

Firstly, investigations were limited to salts based on monovalent ions as the presence of bivalent ions (e.g. Ca^{2+}, Mg^{2+} and SO_4^{2-}) was found to strongly affect the IEMs performance thus resulting into a lower power production [21,22,30,31]. As shown in Table 1, a large number of salts based on monovalent ions was included into the selection procedure to identify a few salt-water solutions to be tested in the experimental campaign.

Table 1: Salts formed by monovalent ions included in the selection procedure. Selected salts are reported in bold-red. Chaotrope ions are indicated in blue. Kosmotrope ions are indicated in black [32].

Cations → **← Anions**	**Li^+**	**Na^+**	**K^+**	**NH_4^+**	**Cs^+**
Cl^-	**LiCl**	**NaCl**	KCl	**NH_4Cl**	CsCl
ClO_3^-	$LiClO_3$	-----	-----	-----	-----
CH_3COO^-	LiOAc	-----	-----	-----	-----
NO_3^- (*)	$LiNO_3$	$NaNO_3$	KNO_3	NH_4NO_3	-----
NO_2^-	$LiNO_2$	-----	-----	-----	-----
Br^-	-----	NaBr	-----	-----	-----

(*) These anions are considered as Chaotrope ions since quite similar ions are considered so in the literature.

Table 1 divides the ions into two different groups: kosmotrope ions and chaotrope ions. In principle, chaotrope ions are featured by large ion radius, single charge and consequently low charge density. Conversely, kosmotrope ions are featured by small ion radius or multiple charge and high charge density. Contrary to what is expected on the basis of the ion radius, the chaotrope ions have a higher mobility in water with respect to the kosmotrope ions. This is due to the fact that the actual ion size in water is much different from the one measured in a crystal: small kosmotrope ions are strongly hydrated and they move bearing several water molecules, while large chaotrope ions are less hydrated thus moving much faster than the kosmotrope ones [33,34]. The classification of the ions in the chaotrope or kosmotrope categories is

based on the value of the Jone and Dole's viscosity coefficient *s* [32], which is present in the equation for the solution relative viscosity:

$$\frac{\eta}{\eta_0} = r\sqrt{C} + sC \quad (1)$$

where η_0 is pure water viscosity at the same temperature and *r* is a constant independent of the concentration *C*.

The kosmotrope ions tend to increase the solution viscosity, 'making the order' in the water structure, thus, they are featured by a positive value of the coefficient *s*. Conversely, the chaotrope ions 'break the order' in the water structure and cause a decrease of the solution viscosity, thus, the coefficient *s* assumes a negative value [32]. Just to give some simplified examples, Cl^-, Br^-, NO_3^-, K^+, NH_4^+ and Cs^+ are generally considered as chaotrope ions, while CH_3COO^-, Li^+ and Na^+ typically belong to the kosmotrope group. Nevertheless, it is worth noting that such differences are not always so clear and it is often easier to define which ion is more chaotrope or more kosmotrope than another one, rather than providing an absolute classification: e.g. potassium, lithium and sodium ions can be ordered as $K^+ < Li^+ < Na^+$ with respect to the kosmotrope properties and in the opposite way with respect to the chaotrope properties.

The salt selection was performed by referring to some properties of the pure salts in water, i.e. (a) *activity coefficients*, (b) *conductivity* and (c) *solubility*.

(a) *Activity coefficients* have a strong influence on the available potential difference across each membrane and therefore on the voltage generated by the stack. (b) Salt solution *conductivity* strongly affects the stack resistance (R_{stack}), which is composed of the electrical resistance of the anionic exchange membranes (R_{AEM}) and cationic exchange membranes (R_{CEM}), the electrical resistance of the dilute and the concentrate compartments (R_{low} and R_{high}) and the blank resistance R_{blank} (i.e. the resistance of the electrodic compartments fed by an appropriate redox couple solution). The term R_{low} is so significant in determining R_{stack} that the conductivity of the salt solution flowing in the dilute compartment is one of the most crucial parameters. (c) Salts *solubility* is another important property: the higher the solubility, the higher the achievable concentration of the solution feeding the concentrate compartment (C_{high}) and thus the higher the salinity gradient available.

Increasing the stack voltage via suitable activity coefficients and concentration ratios across the membranes and decreasing R_{stack} via a suitable solution conductivity results into an enhancement of the RED unit power output.

(a) *Activity Coefficients*

Activity coefficients were evaluated as a function of the salt molality through the Pitzer model for pure salts [35] reported in equations (2-6):

$$f_\gamma = -A_\phi \left[\frac{\sqrt{m_{MX}}}{1 + b\sqrt{m_{MX}}} + \frac{2}{b} \ln(1 + b\sqrt{m_{MX}}) \right] \quad (2)$$

$$B_\gamma = 2\,\beta^{(0)} + 2\,\beta^{(1)} \frac{\left(1 - \left(1 + \alpha\sqrt{m_{MX}} - \alpha^2 \frac{m_{MX}}{2}\right) \exp(-\alpha\sqrt{m_{MX}})\right)}{\alpha^2 m_{MX}} \quad (3)$$

$$C^\gamma = \frac{3}{2}\, C^\phi \quad (4)$$

$$\gamma_{MX} = \gamma_{M^+} = \gamma_{X^-} = \exp\left(f_\gamma + m_{salt}\, B_\gamma + m_{salt}^2\, C^\gamma\right) \quad (5)$$

where:

A_ϕ, α and b are Pitzer's model parameters (values reported in Appendix A only for the salts finally selected);

$\beta^{(0)}$, $\beta^{(1)}$ and C^ϕ are parameters specific for each salt (values reported in Appendix A only for the salts finally selected);

m_{MX} is solution molality;

γ_{cat} and γ_{an} are ions activity coefficients.

The Pitzer model outcomes are reported in Figure 2 for a number of pure salt-water solutions. As it can be seen, the salts including the ion Li^+, such as LiCl, $LiClO_3$ and $LiNO_3$, practically exhibit the highest activity coefficients at any molality.

Interestingly, according to Figure 2, combinations between kosmotrope and chaotrope ions (e.g. LiCl, $LiNO_3$ and NaCl) give rise to salts with higher activity coefficients in water, while salts formed by either two chaotrope (e.g. NH_4Cl, CsCl and NH_4NO_3) or two kosmotrope (e.g. LiOAc) ions exhibit lower activity coefficients. Moreover, the activity coefficient vs. molality trend is found to exhibit a minimum at low molality for the case of salts given by the combination of chaotrope and kosmotrope ions (see in particular Li^+ salts). On the contrary, salts given by the combination of two chaotrope

ions reveal a monotonically decreasing behaviour in the entire range of molality explored. According to the Nernst potential equation [36] (equation 6), the presence of a minimum in the low concentration range should be regarded as an advantage since the lower the activity of the salt-water solution flowing in the dilute compartment, the higher is the resulting electric voltage in the cell pair. Moreover, the value of solution concentrations relevant to these minimum values also guarantee a higher solution conductivity.

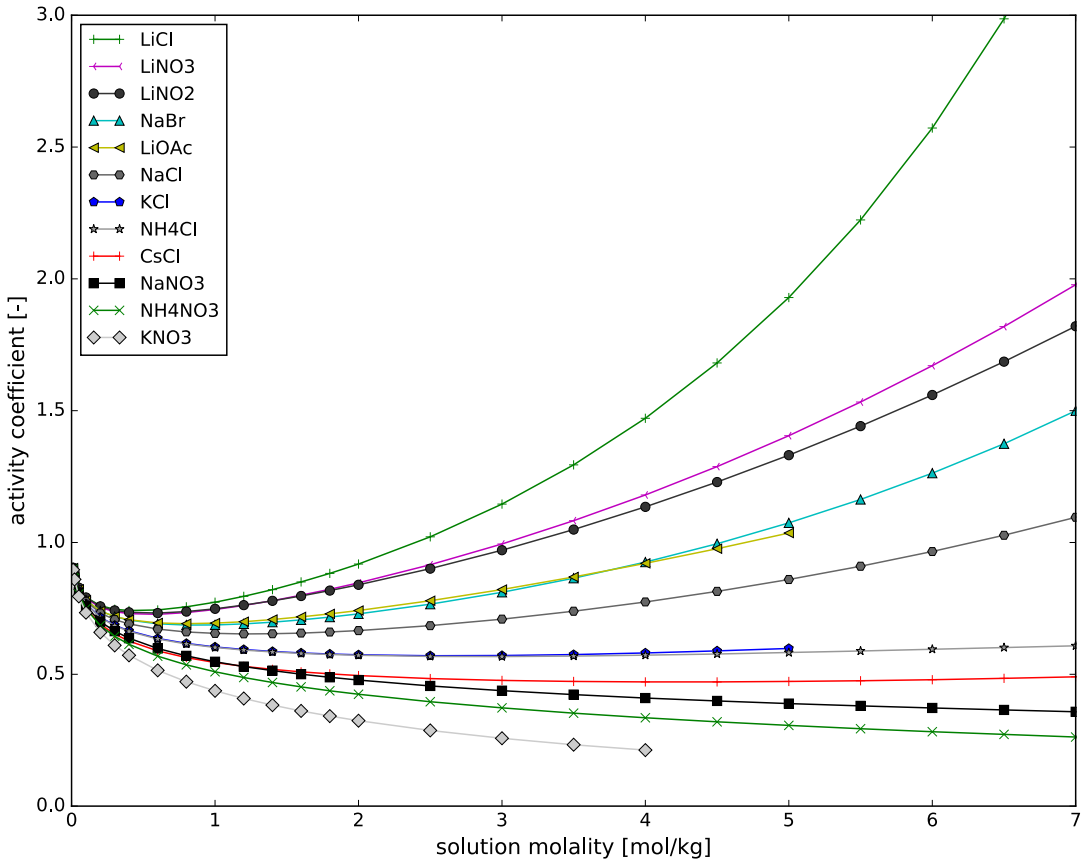

Figure 2: Activity coefficients vs. solution molality for the investigated salts

$$\Delta\phi_{cell} = \frac{RT}{F} ln\left(\frac{a_c^{high} a_a^{high}}{a_c^{low} a_a^{low}}\right) = \frac{2RT}{F} \ln\left(\frac{a_{salt}^{high}}{a_{salt}^{low}}\right) \qquad (6)$$

Some theoretical cell potential difference data relevant to the pure salt-water solutions investigated (see Table 1) are reported in Figure 3 as examples: these were calculated at 25°C, at given concentrations in the dilute and concentrate compartment (i.e. C_{low} = 0.05M and C_{high} = 5M, respectively) and for ideal membranes (i.e. permselectivity α_p =

1). Among the investigated salts, LiCl is shown to provide the highest cell potential difference.

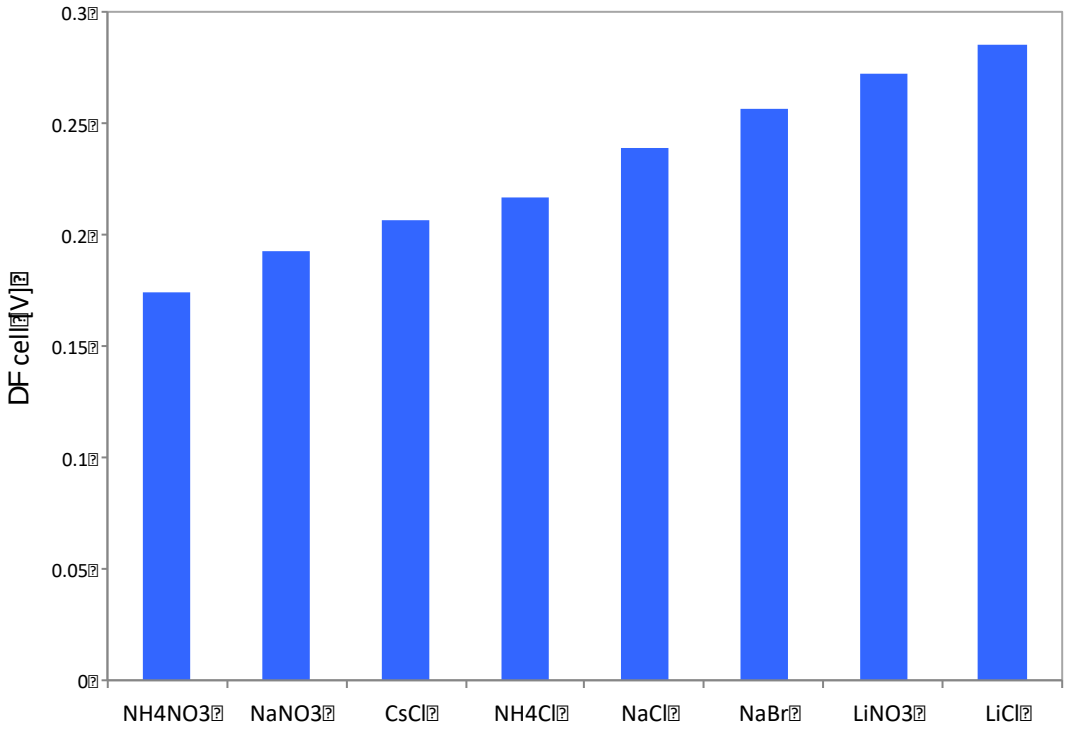

Figure 3. Theoretical cell potential difference with different salts. Calculation conditions: 1 cell pair, C_{high}= 5M, C_{low}=0.05M, T=25°C, α_p=1.

(b) *Conductivity*

Equivalent conductivity at 25°C was calculated with the Jones and Dole's equation [37], whose coefficients are available for a wide range of salts:

$$\Lambda = \Lambda_0 - \frac{A_\Lambda \sqrt{C_{MX}}}{1 + B_\Lambda \sqrt{C_{MX}}} - C_\Lambda C_{MX} \qquad (7)$$

where

Λ_0 is the equivalent conductivity of the salt at infinite dilution (values reported in Appendix 1 for the selected salts only);

A_Λ, B_Λ and C_Λ are parameters specific for each salt (values reported in Appendix 1 for the selected salts only);

C_{MX} is the molarity of the salt.

Figure 4 reports the conductivity values estimated via equation 7 for the salts of Table 1. As it can be seen, NH_4Cl and KCl show the highest conductivity, although the latter has a limited range of solubility (see also next paragraph).

Note that the salts composed of chaotropes ions, as NH_4Cl, KCl and CsCl, exhibit the highest values of conductivity in the entire range of investigated concentrations, while the salts presenting a kosmotrope ion have a much lower conductivity. As a matter of fact, the chaotrope ions are less hydrated and they move faster then the kosmotrope ions, determining a higher conductivity of the electrolyte solution [32]. However, it should be kept in mind that the most enhanced differences are registered at high concentrations, while at lower concentrations, and in particular for concentrations lower than 0.5M, the trends are closer to each other.

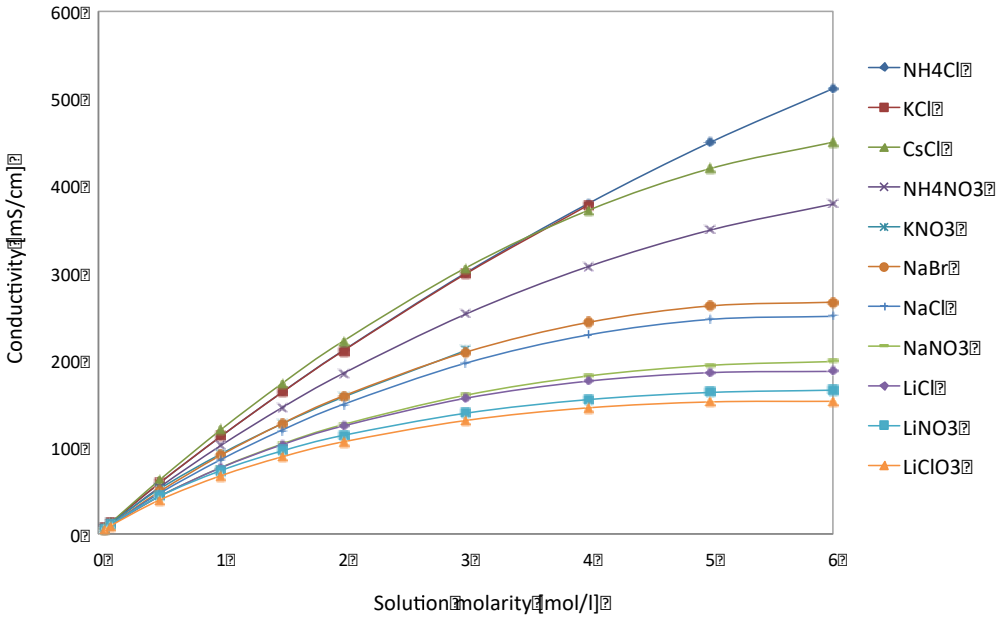

Figure 4: Conductivity vs. solution molarity for the investigated salts with a zoom in the range of concentrations between 0 and 0.5M.

(c) *Solubility*

Solubility data were found in database available in the literature [38,39] (Figure 5). For the purpose of the present work where both pure salt- and salt binary mixture-solutions have to be tested, such data have been employed just to discard all cases exhibiting a solubility in water lower than the NaCl one (which will represent our reference case)

and to have an idea of the potential enhancement achievable at the saturation concentration.

Moreover, it is worth noting that, when the salt saturation point allows to reach higher concentrations, as in the case of LiCl, the corresponding activity coefficients is also greatly enhanced thus ensuring a further enhance of the theoretical cell potential difference.

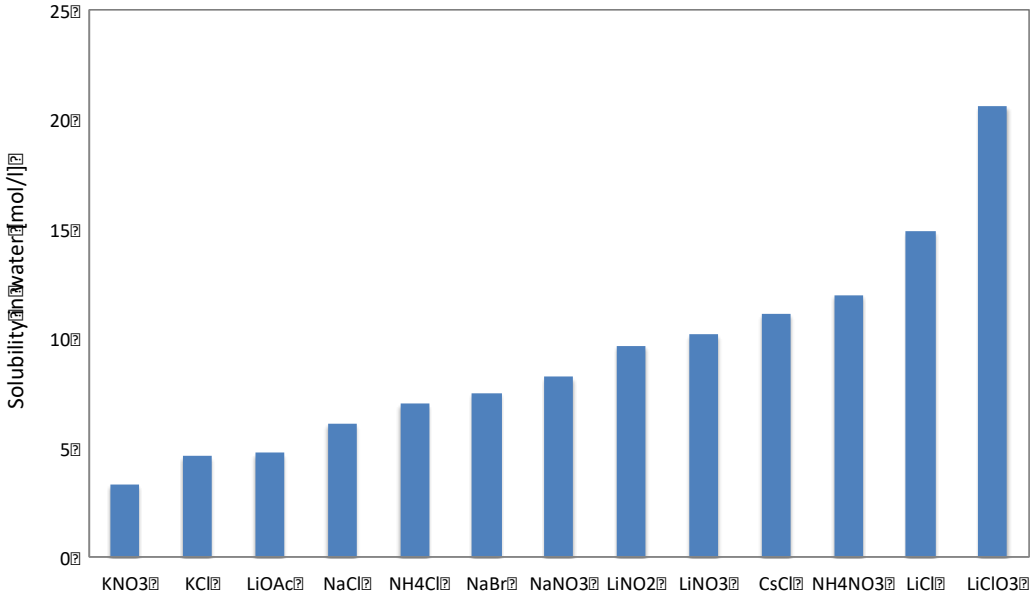

Figure 5. Solubility in water for the investigated salts (T=25°C)

All the information reported above were used to guide the choice of some pure salt-water solution to be tested in the experiments. In particular, on the basis of the activity coefficient along with relevant cell electric potential, the LiCl was considered as the most interesting choice. Similarly, NH_4Cl was judged as the most promising by referring to the solutions conductivity data. NaCl was selected as a reference case as it is the most used and studied salt in RED systems. Note that the above salts where chosen also because they share the same anion thus reducing the number of parameters involved in results explanation. Moreover, both LiCl and NH_4Cl have a solubility higher than the NaCl case thus not representing a limit in the binary mixture tests (see next section). In particular, the really high solubility of LiCl could represent a breakthrough in RED technology potential, as already suggested for the case of Pressure Retarded Osmosis technology [40]. The salts selected for the experimentation are indicated in red-bold in Table 1.

2.2 Salt binary mixture selection

This section is devoted to recognizing which combination of two different salts could enhance the process performance. In order to reduce the high number of possible combinations of Table 1 salts, some assumptions were made:

- considering only binary mixtures of salts in water;
- considering only 50%-50% molar salt mixtures, i.e. each mixture is composed of the same molar amount of the two salts;
- considering only mixtures of salts sharing either the same anion or the same cation.

Following the procedure reported for the pure salt selection, similarly, the selection of the binary mixture was again performed by referring to activity coefficients, conductivity and solubility.

(a) *Activity coefficients*

The activity coefficients of salts in mixture are calculated through the Pitzer model adapted to multicomponent systems [41] which is briefly summarized in the following.

Pitzer's Model

Considering a mixture containing a certain number of ions *i* with a molality equal to m_i and an ionic charge z_i, it is possible to calculate the ionic strength and the modified ionic strength:

$$I = \frac{1}{2}\sum_i m_i z_i^2 \tag{8}$$

$$Z = \sum_i m_i |z_i| \tag{9}$$

Once the ionic strength is known, the interaction parameter f^γ can be assessed as follows:

$$f^\gamma = -A_\phi \left[\frac{I^{1/2}}{1 + b\, I^{1/2}} + \frac{2}{b} \ln\left(1 + b\, I^{1/2}\right) \right] \tag{10}$$

Then, the interaction parameters B_{MX}, B'_{MX} and C_{MX} specific for each salt present in the system can be calculated according to equations (11-13):

$$B_{MX} = \beta^0_{MX} + \left(\frac{\beta^1_{MX}}{\alpha^2 I}\right)\left[1 - \left(1 + \alpha\sqrt{I}\right)\exp\left(-\alpha\sqrt{I}\right)\right] \quad (11)$$

$$B'_{MX} = \frac{2\,\beta^1_{MX}}{\alpha^2\, I^2}\left[-1 + \left(1 + \alpha\sqrt{I} + \frac{1}{2}\alpha^2 I\right)\exp\left(-\alpha\sqrt{I}\right)\right] \quad (12)$$

$$C_{MX} = \frac{C^{\phi}}{2\,|z_M z_X|^{1/2}} \quad (13)$$

where:

$\beta^0_{MX}, \beta^1_{MX}$ are the "observable parameters" typical of each salt (values reported in Appendix 1 for the selected salts only);

α is a constant (value reported in Appendix 1 for the selected salts only);

C^{ϕ} is a parameter specific for each salt (value reported in Appendix 1 for the selected salts only).

A combination of these parameters returns the values of the activity coefficients for each salt present in the solution according to equation 14. In particular, for the generic salt *MX*, the activity coefficient is defined as follows.

$$\begin{aligned}\ln\gamma_{MX} = {} & |z_M\, z_X|\, f^{\gamma} + \left(2\frac{\nu_M}{\nu}\right)\sum_a m_a\left(B_{Ma} + Z\,C_{Ma} + \frac{\nu_X}{\nu_M}\,\phi_{Xa}\right) \\ & + \left(2\frac{\nu_X}{\nu}\right)\sum_c m_c\left(B_{cX} + Z\,C_{cX} + \frac{\nu_M}{\nu_X}\phi_{Mc}\right) + \\ & + \sum_c\sum_a\{+\nu^{-1}[2\,\nu_M\, z_M C_{ca} + \nu_M\psi_{Mca} + \nu_X\psi_{cXa}]\} + \\ & + {}^1\!/_2\sum_c\sum_{c'} m_c m_{c'}\left[\frac{\nu_X}{\nu}\,\psi_{cc'X} + |z_M\, z_x|\,\phi'_{cc'}\right] + \\ & + {}^1\!/_2\sum_a\sum_{a'} m_a m_{a'}\left[\frac{\nu_M}{\nu}\psi_{Maa'} + |z_M\, z_x|\phi'_{aa'}\right]\end{aligned} \quad (14)$$

where

c is the index used for the cations present in the solution;

a is the index used for the anions present in the solution;

ν_M and ν_X are the cation and anion stoichiometric coefficients respectively, both equal to 1 for uni-univalent salt;

z_M and z_X are the cation and anion charge respectively;

B_{Ma} and C_{Ma} are the second order interaction parameters relevant to the salt composed of the the cation M^+ and a generic anion *a*;

B_{cX} and C_{cX} are the second order interaction parameters relevant to the salt composed of the the anion X^- and a generic cation *c*;

B'_{ca} is the interaction parameter between the generic anion and cation;

ϕ_{Mc} is the second order interaction coefficients between the cation M^+ and the other generic cation *c*;

ϕ_{Xa} is the second order interaction coefficients between the anion X^- and the other generic anion *a*;

$\phi_{cc'}$ is an interaction parameter between two different cations, usually set equal to zero;

$\phi_{aa'}$ is an interaction parameter between two different anions, usually set equal to zero;

ψ_{Mca} is the third order interaction parameter among the cation M^+, a generic cation *c* and a generic anion *a*;

ψ_{Xac} is the third order interaction parameter among the anion X^-, a generic cation *c* and a generic anion *a*.

According to Pitzer's model, the activity coefficient of a pure salt in water is modified when mixed with another salt in the same solution due to interaction forces. In particular, for all the salts (and all possible binary mixtures) tested in the present work, their γ_{MX} as pure compound in water, can exhibit either an enhancement or a reduction when mixed with another salt depending on the $\gamma_{M'X'}$ of the latter as pure compound in water. More precisely, when $\gamma_{MX} < \gamma_{M'X'}$, $\gamma_{MX,mix}$ will be higher than γ_{MX}, while $\gamma_{M'X',mix}$ will be lower than $\gamma_{M'X'}$. This model outcome is shown in Figure 6 for the case of a 50%-50% mixture of NH_4Cl-LiCl: as it can be observed in the figure, since $\gamma_{NH_4Cl} < \gamma_{LiCl}$, $\gamma_{NH_4Cl,mix} > \gamma_{NH4Cl}$, while $\gamma_{LiCl,mix} < \gamma_{LiCl}$.

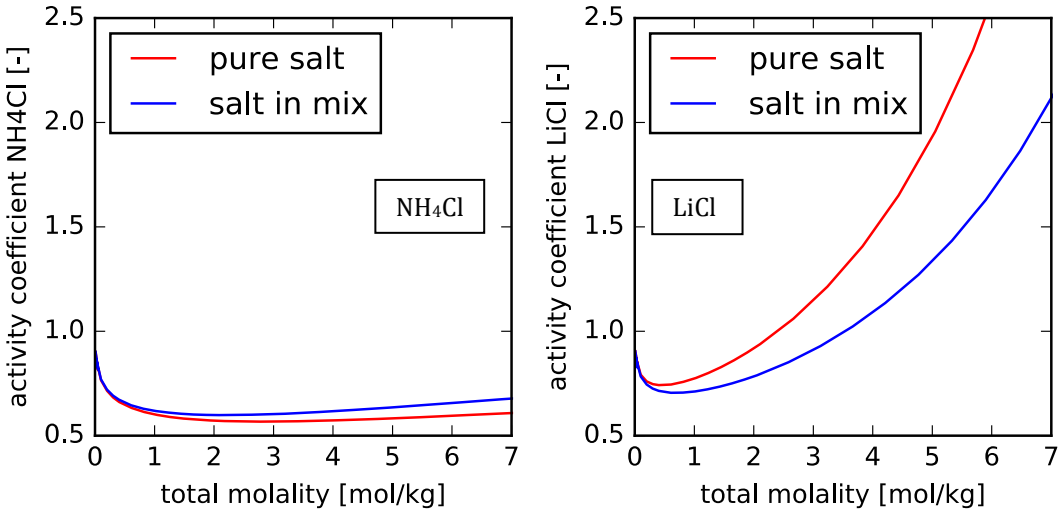

Figure 6. Activity coefficients of NH_4Cl (left) and LiCl (right) in water vs solution molality as pure salts and in 50%-50% NH_4Cl-LiCl mixture.

As already discussed for the pure salt cases, once activity coefficients of ions in water have been calculated, the cell potential difference can be assessed. For binary salt mixtures and ideal membranes (i.e. permselectivity α_p=1), the multicomponent Nernst equation reported in [42,43] was derived as follows:

$$\Delta\phi_{cell} = \frac{RT}{2F}\, ln\left(\frac{a_{c1}^{high} a_{c2}^{high} a_{a1}^{high} a_{a2}^{high}}{a_{c1}^{low} a_{c2}^{low} a_{a1}^{low} a_{a2}^{low}}\right) = \frac{RT}{F}\ln\left(\frac{a_{salt1}^{high} a_{salt2}^{high}}{a_{salt1}^{low} a_{salt2}^{low}}\right) \qquad (15)$$

where the number 2 visible at the denominator is relevant to the number of salts present in the solution.

Figure 7 shows the ideal cell potential difference calculated (i) for some of the analysed salt binary mixture-water solutions and (ii) for the corresponding pure salt-water solutions at a given operating condition (i.e. C_{high} = 5M and C_{low} = 0.05M, T=25°C, α_p=1). As expected on the basis of the activity coefficients found for the salts in the mixtures, the mixture-$\Delta\phi_{cell}$ is found included in the range between the two pure-$\Delta\phi_{cell}$ cases. Notably, in many cases the mixture-$\Delta\phi_{cell}$ results closer to the lowest pure-$\Delta\phi_{cell}$.

However, the salt mixtures with LiCl are shown to provide the highest mixture-$\Delta\phi_{cell}$ thanks to the high γ_{LiCl} as pure salt in water: in particular its mixtures with NH_4Cl and NaCl appear as the most promising among those sharing the same anion.

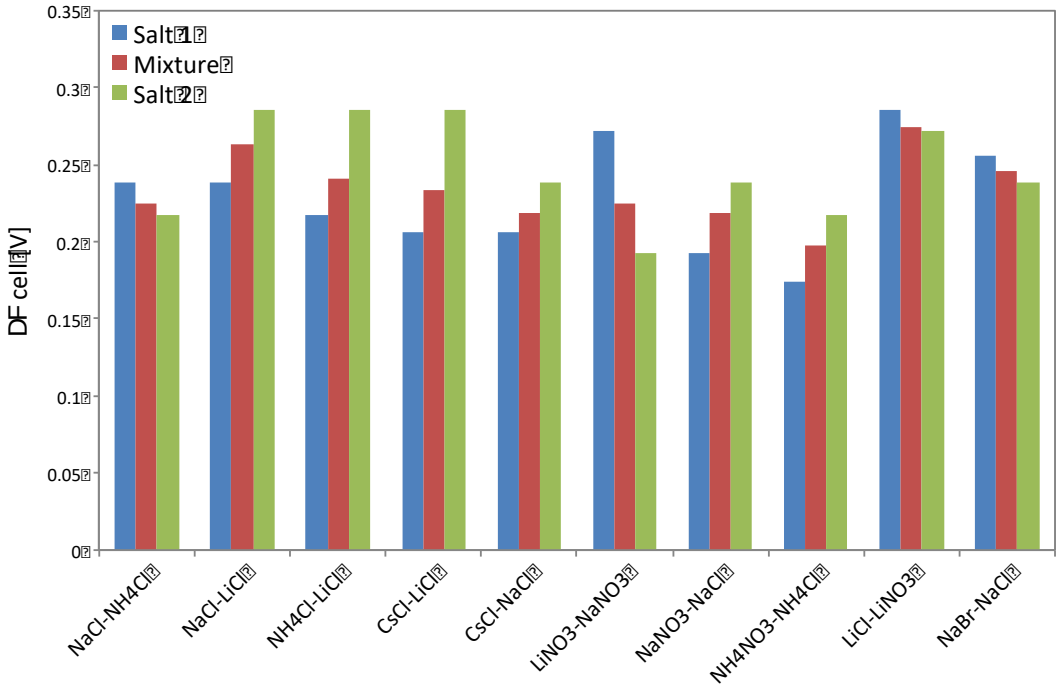

Figure 7. Theoretical cell potential difference values calculated for binary 50%-50% mixture-water solutions and for corresponding pure salt-water solutions (C_{high} =5M; C_{low} =0.05M, ideal membranes: α=1).

(b) *Conductivity*

The conductivity of the two salt-water solutions was measured via some purposely made laboratory experiments (see for instance section 4.2). As expected, the values were found to be intermediate between the two pure salt-cases. Following this evidence, the solutions including the NH_4Cl are expected to be able to mostly reduce the stack electrical resistance.

(c) *Solubility*

Given the fact that the salt mixtures investigated include salts sharing either the same anion or the same cation, considerations concerning the solubility strictly follow those already discussed for the pure salt cases: mixture including salts whose solubility is lower than the NaCl one were discarded in the selection.

On the basis of the findings of this section 2.2 and also following the selection already made for the pure salt-water cases (section 2.1), it was decided to investigate binary

mixture composed of the salts selected in section 2.1, i.e. NaCl-LiCl, NaCl-NH_4Cl, NH_4Cl-LiCl.

3. EXPERIMENTAL

3.1. Experimental apparatus

The lab-stack (manufactured and provided by REDstack BV) used for the experiments reported in this work is composed of 5 cell pairs, each one consisting of two channels where the solutions at different concentration are forced to flow. These channels are separated by Fujifilm® membranes (E1 type, thickness of 250 μm): an anionic exchange membrane (AEM) and a cationic exchange membrane (CEM) whose area is equal to $0.1 \times 0.1 m^2$. Channel dimensional stability and flow mixing enhancement within them are guaranteed by 150μm-woven-spacers provided by Deukum®.

The experimental apparatus (Figure 8) is composed of the RED unit, two bottles containing the concentrate and dilute feed solutions forced to circulate within the stack by two peristaltic pumps (by MasterFlex Cole-Parmer®), two bottles in which the outlet solutions are collected and a tank containing the electrode-rinse solution recirculating in a closed-loop thanks to another peristaltic pump.

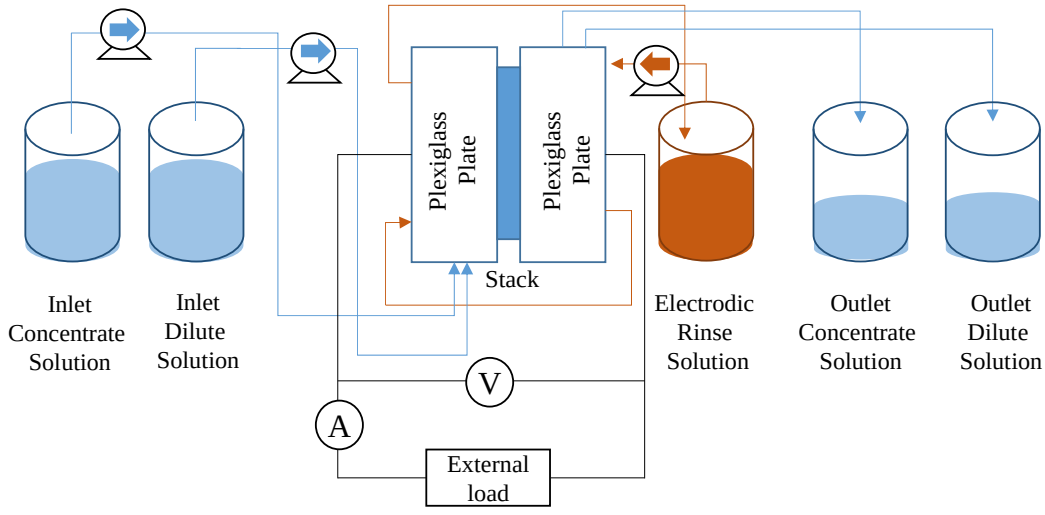

Figure 8. Scheme of the experimental apparatus employed for the experiments.

Inside the stack the ions tend spontaneously to migrate from the concentrate solution to the adjacent dilute ones, in particular the cations pass through the CEMs and the anions through the AEMs. This migration gives rise to a current of ions inside the stack,

towards the electrodes placed at the ends of the stack: the cations migrate toward the cathode and the anions toward the anode. At the electrodes, where a suitable electrodic rinse solution circulates, the ionic current is converted into electric current through redox reactions [7], which circulate in the external circuit to supply the external load.

Note that the redox couple hexacyanoferrate(III)/hexacyanoferrate(II) $[Fe(CN)_6]^{4-}$ /$[Fe(CN)_6]^{3-}$ was employed in the experiments as it was judged as suitable for RED applications, thanks to its very high stability (in absence of light and oxygen) and very low toxicity [44]. The electrodic solution contains also 0.25 moles per liter of NaCl, as supporting electrolyte. The two ends of the stack are connected to a variable external load (by Sfernice®). The external circuit contains also an amperometer (by Fluke®) in series with the stack and a voltmeter (by Fluke®) in parallel, in order to read the current and the voltage, respectively, corresponding to the imposed external load.

The employed solutions and operating conditions investigated throughout the present work are shown in Table 2. Notably, different values of C_{high} were tested because in a RED closed-loop arrangement, the regeneration unit thermal duty is expected to be lower, the lower C_{high}, possibly resulting into a higher cycle efficiency.

Table 2. Summary of the experiments carried out in the present work

		$v_{low}=v_{high}$ [cm/s]	C_{low} [mol/l]	C_{high} [mol/l]
Pure salts	NaCl	0.5; 1; 2	0.05	0.5; 2; 5
	NH_4Cl	0.5; 1; 2	0.05	0.5; 2; 5
	LiCl	0.5; 1; 2	0.05	0.5; 2; 5
Salt mixtures	NaCl-NH_4Cl	2	0.05	0.5; 2; 5
	NH_4Cl-LiCl	2	0.05	0.5; 2; 5
	NaCl-LiCl	2	0.05	0.5; 2; 5

3.2. Methodology

Each experiment concerns the measurements of the voltage and of the current density across the stack as a function of the resistance of the external load (R_u).

The threshold values reported in Figure 9 are represented (i) by the *open circuit condition* where the external load is not connected (i.e. R_u approaches infinity) and the voltage measured is the Open Circuit Voltage (OCV) and (ii) by the *short circuit condition* where $R_u = 0$. Clearly, the lower R_u, the lower the measured voltage and the higher the measured current density. Plotting the voltage against the current density results in a trend, which is linearly decreasing (equation 16).

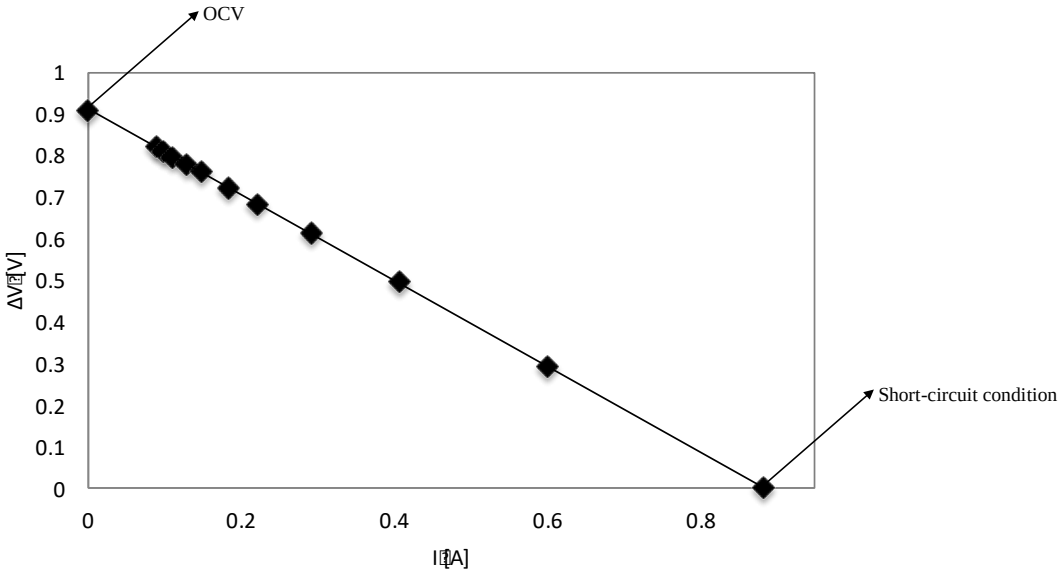

Figure 9. Trend of the stack voltage versus electric current for the case of NaCl-water solutions. Operating conditions: 5 cell pairs-stack, A=0.1×0.1m^2, C_{low}=0.05M, C_{high}=5M, v_{low}=v_{high}=2 cm/s, T=25°C.

$$\Delta V = OCV - R_{stack} I \tag{16}$$

The slope of this trend gives the value of the stack resistance.

Once the values of current density and voltage are known, it is possible to calculate the corresponding values of Power Density P_D (equation 17):

$$P_D = R_u \cdot I^2 = \Delta V \cdot I = \Delta V \frac{OCV - \Delta V}{R_{stack}} = -\frac{\Delta V^2}{R_{stack}} + \frac{OCV \cdot \Delta V}{R_{stack}} \tag{17}$$

The parabolic P_D vs. ΔV trend results into a P_D = 0 for ΔV = 0 and ΔV = OCV and P_D equal to its maximum for ΔV = OCV/2. The maximum of P_D-ΔV trend corresponds to the condition in which the imposed R_u is equal to R_{stack}. This condition will be adopted in all the experiments carried out.

Just as an example, in Figure 10 the P_D versus ΔV trend is reported for the case of NaCl-water solutions: at a given solutions velocity (v_{low}=v_{high}=2 cm/s) and dilute compartment concentration (C_{low} = 0.05M), three different concentrations of the concentrate solutions were tested (C_{high} = 0.5M, 2M, 5M). Clearly, in the investigated range of concentrations, the higher the salinity gradient available across the membranes, the higher the resulting P_D. The above described procedure will be adopted

for all the experiments summarized in Table 2. All experiments were carried out twice and very similar results were obtained thus guaranteeing a good reliability of the experimental procedure: in particular, discrepancies between variables measured in two runs of the same experiment were found always lower than 6%.

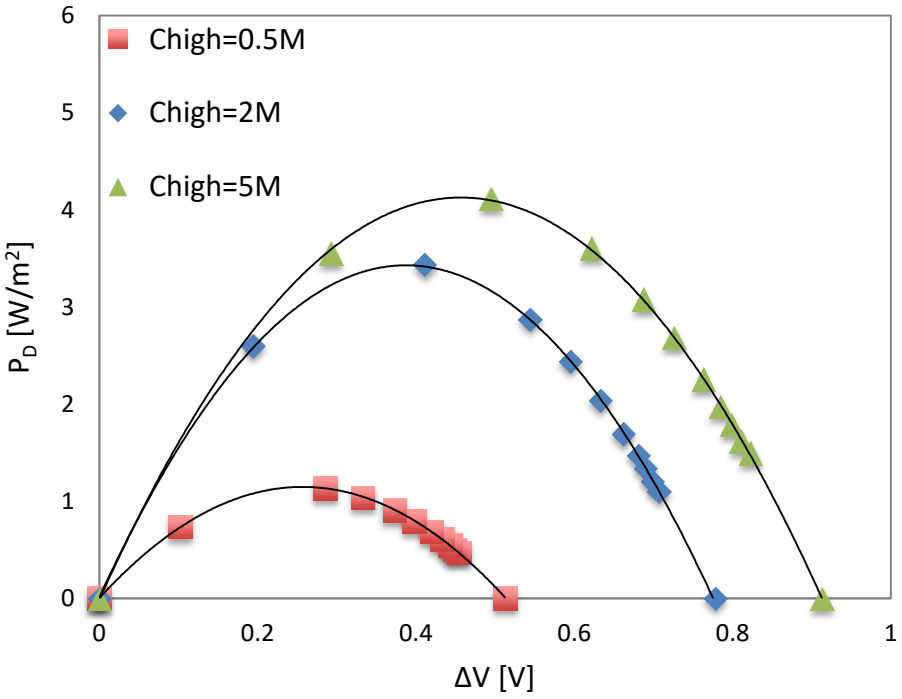

Figure 10. Experimental trends of Power density vs stack voltage for the case of NaCl-water solutions. Operating conditions: 5 cell pairs-stack, A=0.1×0.1m^2; C_{low}=0.05M; C_{high}=0.5M, 2M, 5M; v_{low}=v_{high}=2 cm/s, T=25°C.

The Stack Resistance R_{stack}, which can be inferred from the ΔV *vs* I line, can be considered as the sum of five different resistances:

$$R_{stack} = R_{blank} + N_{cell}\left(R_{low} + R_{high} + R_{AEM} + R_{CEM}\right) \qquad (18)$$

where R_{blank} is the electric resistance of the electrodic compartment, R_{AEM} is the resistance of the AEM, R_{CEM} is the resistance of the CEM, R_{high} is the resistance of the concentrate compartment, R_{low} is the resistance of the dilute compartment [45], N is the number of cell pairs.

Note that the higher the number of cell pairs, the lower the impact of R_{blank} on R_{stack}: in particular, this value is well known to be negligible for the case of large scale stacks. It is not the case for lab-scale measurements as those carried out in the present work, thus requiring the R_{blank} value to be assessed. In order to do so, a suitable stack containing

only one cation exchange membrane and fed by the above mentioned electrodic solution only was employed. By imposing an increasing voltage and measuring the corresponding electric current as shown in Figure 11, R_{blank} can be assessed as the slope of the resulting linear trend and was found equal to 0.0327 Ωm^2.

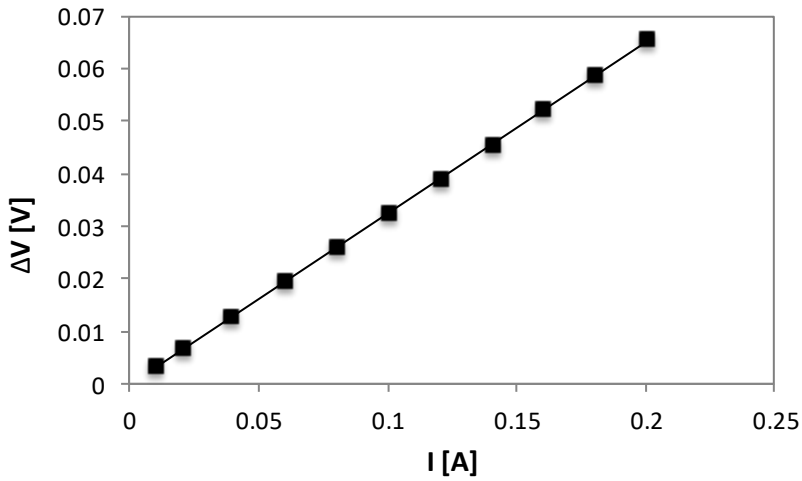

Figure 11. Imposed voltage vs. measured electric current for a stack composed of one CEM only and fed by the electrodic solution (containing the redox couple $[Fe(CN)_6]^{4-}/[Fe(CN)_6]^{3-}$ at a concentration of 0.1M and NaCl as supporting electrolyte at a concentration of 0.25M), T=25°C, A=0.1×0.1m^2.

Once the value of R_{blank} is known, it is possible to correct the measured value of P_D as reported in equation 19 where $P_{D,corr}$ represents the power density obtainable for a large number of cell pairs (as in a full scale stack) where R_{blank} contribution is negligible and $R_u = R_{stack}$.

$$P_{D,corr} = \left(\frac{OCV}{2\,R_{stack} - R_{blank}}\right)^2 \frac{R_{stack}}{N_{cell}\,A} \qquad (19)$$

4. RESULTS AND DISCUSSION

4.1. Experiments with pure salts

The three salts selected in section 2.1 were tested in RED unit experiments according to the procedure described in section 3: as already shown in Figure 10, in these experiments C_{low} was kept constant while three different values of C_{high} were tested. Figure 12 shows, for each pure salt-water solution, the effect of solution velocity (set equal in all compartments) and C_{high} on the main figures of a RED unit: *OCV*, R_{stack} and $P_{D,corr}$.

Independently of the pure salt taken into account, similar dependences of *OCV*, R_{stack} and $P_{D,corr}$ on solution velocity were found. In particular, *OCV* always is shown to increase with the velocity while R_{stack} in most cases decreases as the velocity increases (Figure 12). These cooperative effects clearly results into a $P_{D,corr}$ increase with *v*. *OCV* increase with *v* is due to the lower solution residence time within the stack: the lower the residence time, the lower the concentration change along the channels thus resulting into a driving force, which poorly reduces in the streamwise direction [24]. This phenomenon has an effect also on R_{stack}, and in particular on the overall of the dilute channel R_{dil} which, at low C_{low}, often is the main contribution to R_{stack}. More precisely, solution velocity mainly affects both the ohmic and non-ohmic contributions to R_{dil} [2,46], respectively. The former is again related to the streamwise variation of the concentration along the compartment: practically, the lower *v*, the higher the concentration streamwise increase which yields a lower mean-R_{dil}. Conversely, the non-ohmic contribution is due to the cross-stream concentration change relevant to the boundary layer: clearly, the higher the flow rate within the channel, the higher the cross-stream velocity components, which can reduce the polarization effect [47]. The slightly decreasing R_{stack} vs *v* trend shown in Figure 12 suggests that the effect of *v* on R_{BL} is prominent with respect to that on the ohmic contribution, as expected on the basis of the low channel thickness investigated in the present work [48]. Clearly, as it can be seen in Figure 12, *OCV*, R_{stack} and $P_{D,corr}$ are approaching a plateau as *v* increases as expected: this occurs because at high *v* the mixing within the channel is highly enhanced thus resulting into really low concentration gradients throughout each channel. Based on these above considerations a velocity of 2cm/s was adopted for all the other experiments.

Figure 12 shows also the effect of C_{high} on *OCV*, R_{stack} and $P_{D,corr}$. *OCV* is higher as C_{high} increases due to a higher driving force. Conversely, R_{stack} generally decreases as C_{high} increases for NH_4Cl and LiCl, while a decreasing-increasing behaviour is observable for NaCl, as already found in other literature works [49,50]. Notably, although much less evident, the same behaviour was also observed for NH_4Cl at v=2cm/s. This decreasing-increasing trend can be explained by referring to R_{low} and R_{IEM} only, since R_{high} is negligible. R_{low} is known to decrease as C_{high} increases due to a larger amount of ions crossing the membranes. The membranes are in contact with solutions at different concentrations and their electrical resistance is determined by both the two solutions, although some studies demonstrated that the effect of the dilute solution is prominent [51,52]. The membrane resistance can be considered as the equivalent of two resistances in series: i.e. the one of the micro pores in which the solution flows and the other of the gel phase, which depends on the membrane swelling degree. The former is a decreasing function of the external solution concentration, while the latter increases at larger external solution concentration [49]. Summarizing, these competitive effects coupled with the concentration effect on R_{low} may or may not lead to a minimum in the R_{stack} - C_{high} trend, depending on which are the main contributions to R_{stack}.

The combination of the effects of C_{high} on *OCV* and R_{stack} results into an increase of $P_{D,corr}$ as C_{high} is increased.

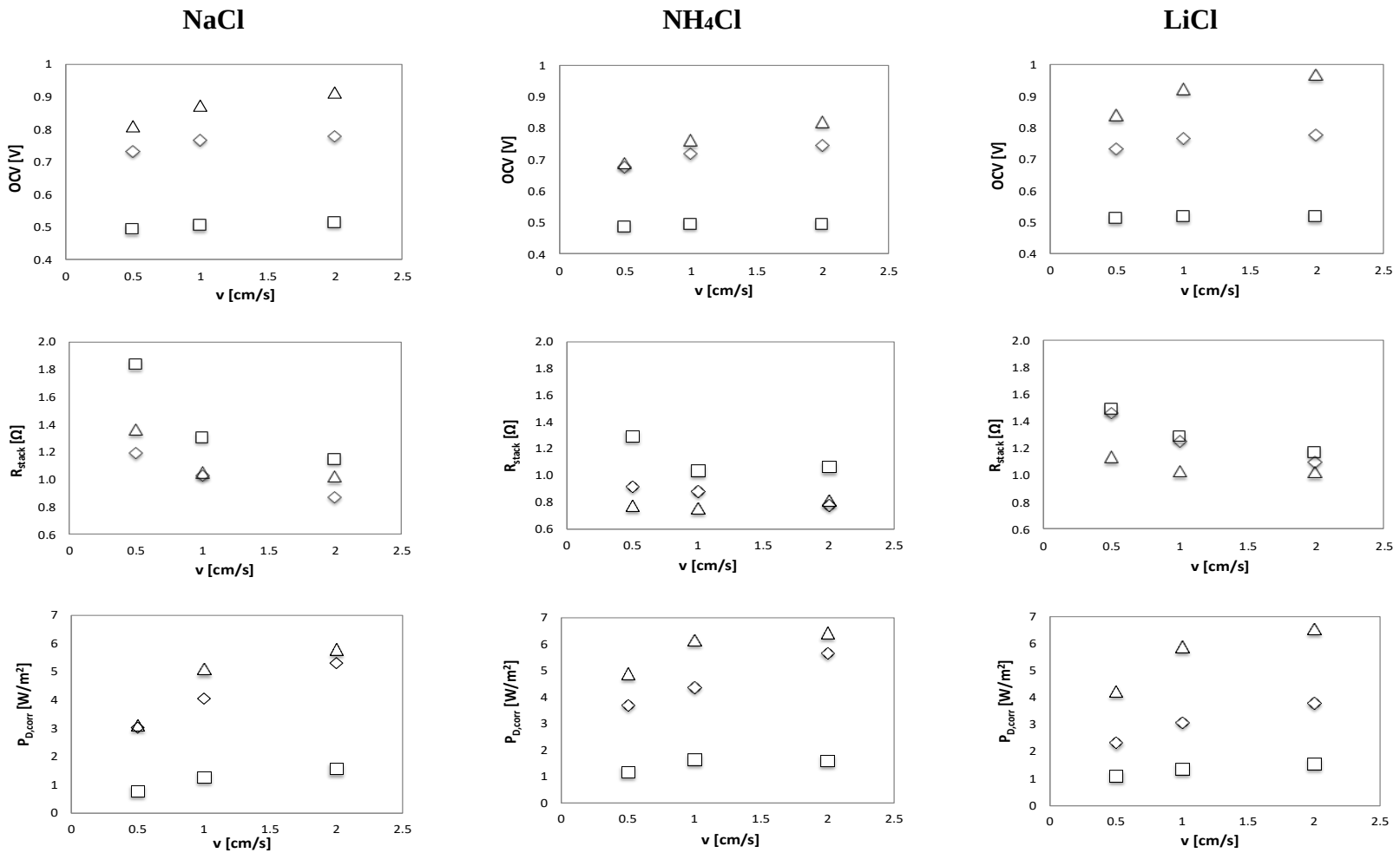

Figure 12 . Experimental *OCV*, R_{stack} and $P_{D,corr}$ as functions of C_{high} and *v*. 5 cell pairs stack fed with solutions of NaCl (left column), NH_4Cl (middle column) and LiCl (right column), A=0.1×0.1m^2; C_{low}=0.05M; C_{high}=0.5M (□), 2M (◊) and 5M (Δ); v_{low}=v_{high}=0.5 cm/s, 1 cm/s and 2 cm/s; T=25°C.

Figure 13 shows *OCV*, R_{stack} and $P_{D,corr}$ values for the three salts at a given solution velocity (v = 2cm/s) for comparison purposes.

As regards the *OCV* values, it is possible to observe that the highest *OCV* was obtained for LiCl solutions especially at high C_{high}, followed by NaCl, while NH_4Cl exhibits the lowest values. This hierarchy is a direct consequence of the activity coefficients of these salts already reported in Figure 2, somehow confirming the outcomes of the Pitzer model for the pure salt-water solutions. However, it is worth noting that the difference between NaCl and LiCl is not as high as expected because of membrane permselectivity effects: in fact, IEMs are optimized to deal with NaCl-water solutions, thereby exhibiting lower permselectivity for the case of LiCl.

R_{stack} values reported in Figure 13 somehow confirms the hierarchy observable in the conductivity data of Figure 4: being NH_4Cl-water solutions the most conductive, corresponding measured R_{stack} were the lowest at any C_{high}.

As it concerns $P_{D,corr}$, it is not possible to recognize a pure salt-water solution able to provide the highest $P_{D,corr}$ at any C_{high}. At C_{high}=0.5M and 5M, the lower R_{stack} exhibited by NH_4Cl-water solutions and the higher *OCV* typical of LiCl ones somehow counterbalance each other thus yielding similar $P_{D,corr}$ values. Conversely, the really higher R_{stack} value observable at C_{high}=2M for LiCl leads to the lowest $P_{D,corr}$.

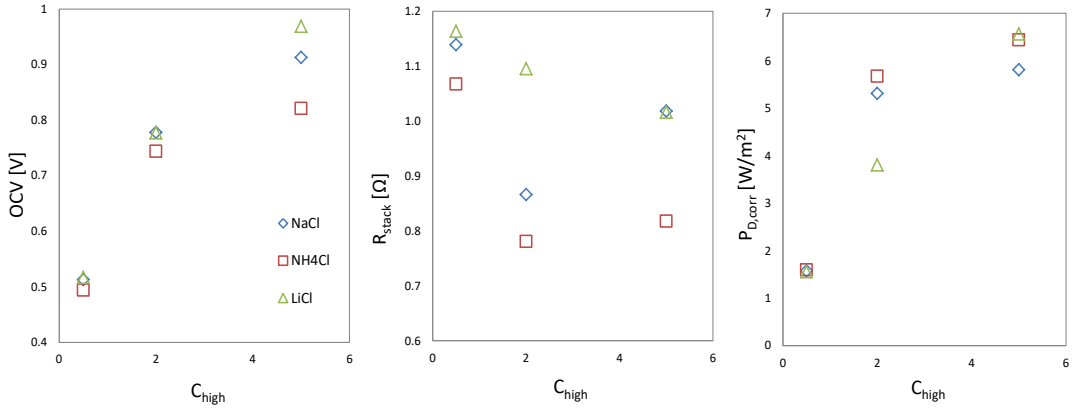

Figure 13. *OCV*, R_{stack} and $P_{D,corr}$ for the three different salts (NaCl, NH_4Cl or LiCl) at different C_{high}. 5 cell pairs stack; A=0.1×0.1m^2; C_{low}=0.05M; C_{high}=0.5M, 2M and 5M; v_{low}=v_{high}=2 cm/s; T=25°C.

On overall, on the basis of the results collected here with Fujifilm IEMs (optimized for NaCl), the use of NH_4Cl is suggested in the range of C_{high} investigated, while better performance in terms of power production are expected with the use of LiCl at larger C_{high} (i.e. C_{high} >6M not investigated in the present work).

4.2. Experiments with mixture of salts

Water solutions prepared with the three salts mixture selected in section 2.2 were used as feed in the RED unit experiments described in the present section.

The mixture selection was performed by assuming that the binary mixture-water solutions conductivity was intermediate between the two pure salt-water cases. This assumption was validated by purposely performed measurements reported in Figure 14. As it is shown in the figure, binary mixture-water solutions conductivity was always found about midway between the conductivities of the two pure salt-solutions.

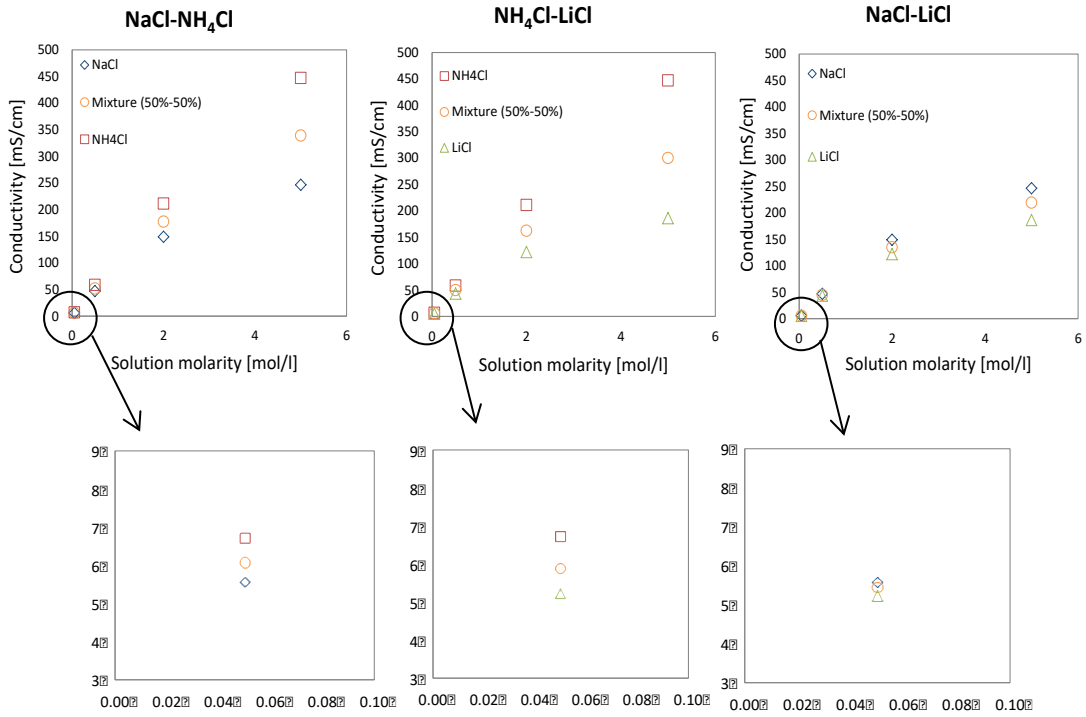

Figure 14. Experimental values of the conductivity obtained with the mixtures and with the corresponding pure salts at different concentrations (0.05M; 0.5M; 2M; 5M), temperature of 25°C. The conductivity values for the case of solution concentration equal to 0.05M are zoomed in the graphs below.

All the experiments with salt mixtures (summarized in Table 2) reported in the following figures were carried out by adopting the same procedure described in section 3.

In Figure 15 the *OCV* values obtained with the salt mixtures are compared with the corresponding ones relevant to the pure salts solutions.

The *OCV* values measured in the salt binary mixture-water solutions are always included between the *OCVs* of the two corresponding pure salt-water solutions. From a close inspection of the figure, it can be inferred that the mixture-*OCVs* are a bit closer to the lowest pure-*OCVs*. This experimental evidence somehow confirms the theoretical

analysis outcomes, where a similar behaviour was observed both in the activity coefficient prediction and in the *OCV* values calculated.

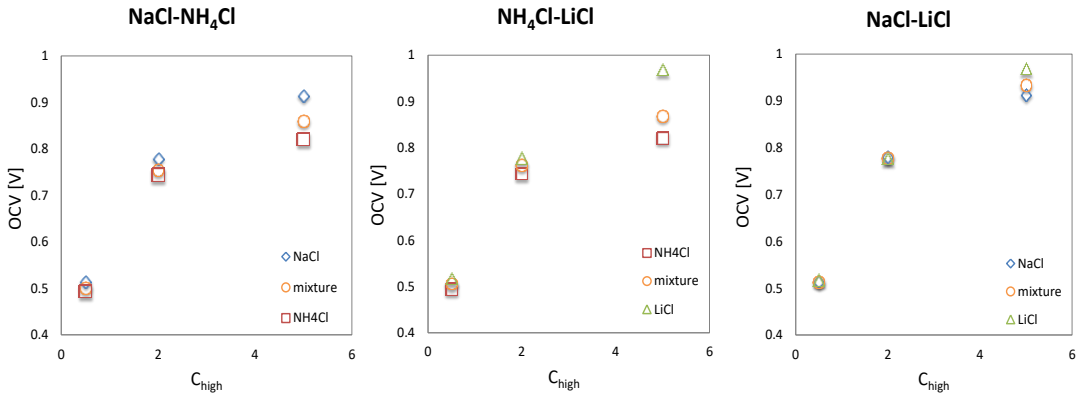

Figure 15. Comparison of the experimental values of *OCV* obtained with the mixtures and with the corresponding pure salts at different C_{high}. Stack composed of 5 cell pairs; A=0.1×0.1m^2; C_{high} =0.5M, 2M, 5M; C_{low} =0.05M; v_{low}=v_{high}=2 cm/s; T= 25°C.

Results concerning the measurement of R_{stack} for the salt mixture-water solution are shown in Figure 16, where a comparison with R_{stack} values measured with the pure salt cases is also provided.

The three mixtures present an analogous behaviour: quite surprisingly, when C_{high} is equal to 0.5M and 5M, the R_{stack} measured for the salt binary mixture is lower than both the two values measured for the pure salts. This finding probably derives from a complex interaction among ions, water and membrane fixed charges [49] and it is not easy to provide a robust explanation for this phenomenon only on the basis of the results here collected. In all the experiments carried out in the present work, the average R_{IEM} is always the most significant contribution to R_{stack}. In particular, the R_{stack} reduction encountered is allegedly due to a reduction of R_{CEM} that may result from an enhanced cation transport inside the pores. It is like that the transport of one cation type inside the pores was enhanced thanks to the presence of the other and vice-versa. Practically, the presence of a second cation modifies the above complex interaction: according to Geise et al. [53] the presence of cations with large binding affinity (as Na^+ and NH_4^+) may enhance the passage of other cations due to a fixed-charge concentration reduction and a consequent Donnan exclusion weakening. The above reduction of R_{stack} measured in the salt mixture with respect to the pure salt was not recognized at C_{high} = 2M. This different behaviour at 2M may be linked to the fact that at this concentration a minimum in R_{stack} - C_{high} trend was observed for the pure salt cases.

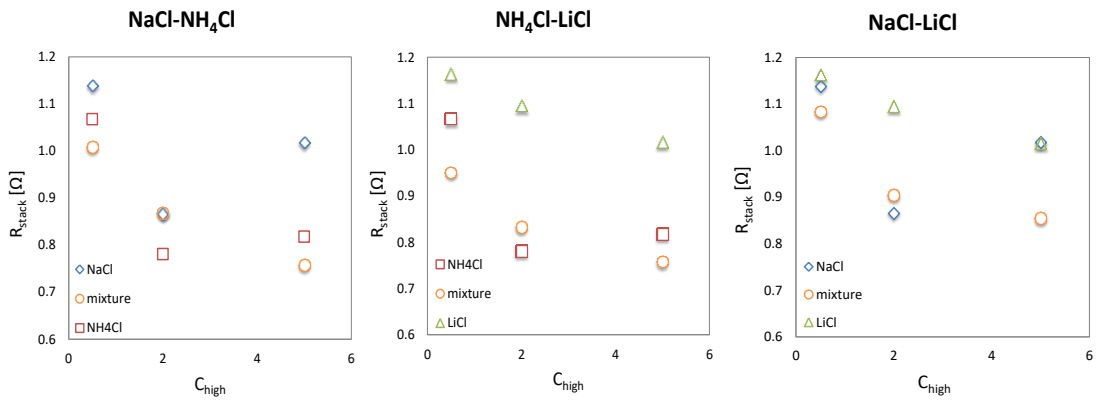

Figure 16. Comparison of the experimental values of R_{stack} obtained with the mixtures and with the corresponding pure salts at different C_{high}. Stack composed of 5 cell pairs; A=0.1×0.1m^2; C_{high} =0.5M, 2M,5M; C_{low} =0.05M; v_{low}=v_{high}=2 cm/s; T= 25°C.

The above discussed surprising reduction of R_{stack} with the salt binary mixtures leads to a $P_{D,corr}$ being higher than both those relevant to the two pure salts at C_{high} =0.5 and 5M as shown in Figure 17. It is worth observing that, according to the findings reported in this figure, it is possible to increase the power produced by a RED unit operating under typical conditions (i.e. NaCl-water solutions, C_{low} =0.05M, C_{high} =0.5M (seawater) or 5M (brine), v_{low} = v_{high} = 2 cm/s) just by adding an equivalent molar quantity of another salt as LiCl or NH_4Cl.

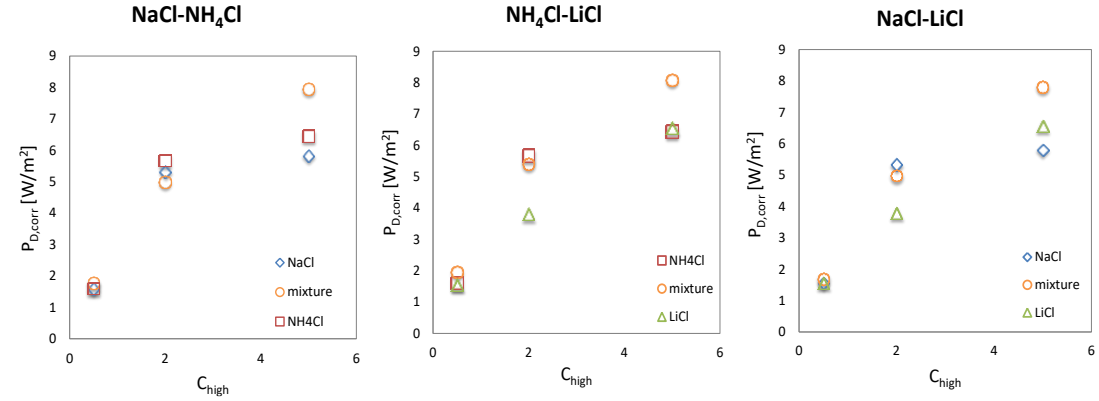

Figure 17. Comparison of the experimental values of $P_{D,corr}$ obtained with the mixtures and with the corresponding pure salts at different C_{high}. Stack composed of 5 cell pairs; A=0.1×0.1m^2; C_{high} =0.5M, 2M, 5M; C_{low} =0.05M; v_{low}=v_{high}=2 cm/s; T= 25°C.

Finally, in Figure 18 the measured values of *OCV*, R_{stack} and $P_{D,corr}$ for the three binary mixtures are reported for comparison purposes.

As concerns the *OCV*, the NaCl-LiCl mixture exhibits the highest values, as expected since the activity coefficients of the two pure salts in water are much higher than the NH_4Cl ones. On the other hand, the NaCl-LiCl mixture yields the largest R_{stack} as it does

not contain the NH_4Cl salt, which exhibits the highest conductivity in water. These opposite properties provided by the binary salt mixtures investigated lead to a $P_{D,corr}$ similar for the three cases independently of C_{high}, although the NH_4Cl-LiCl mixture appears as the most promising.

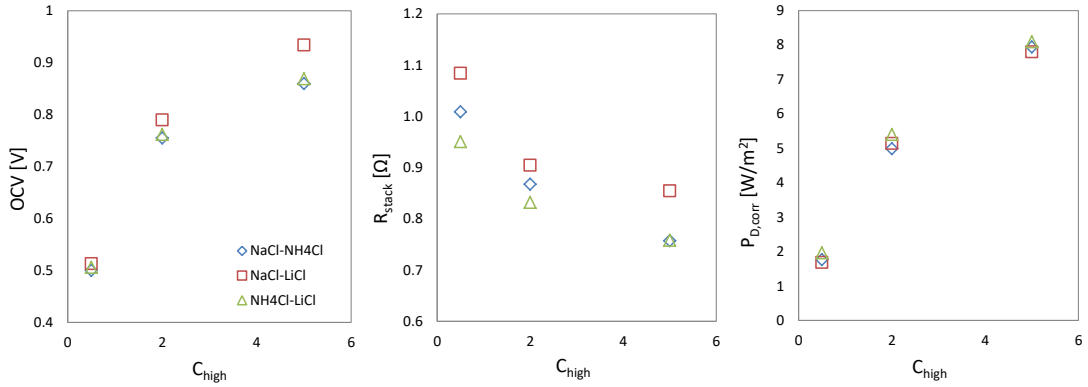

Figure 18. Comparison of the values of *OCV* (left graph), R_{stack} (middle graph) and $P_{D,corr}$ (right graph) for the mixtures NaCl-NH_4Cl, NaCl-LiCl and NH_4Cl-LiCl (stack composed of 5 cell pairs; C_{high}=0.5M, 2M, 5M; C_{low}=0.05M; v_{high}=v_{low}=2cm/s; T=25°C; A=0.1×0.1m^2).

CONCLUSIONS

In the present work the behaviour of non-conventional aqueous solutions of pure uni-univalent salts and salt equimolar binary mixtures in a Reverse Electrodialysis Unit was investigated via experiments. The idea was that of enhancing the power produced by a RED unit to be employed within a closed-loop arrangement to convert low-grade heat into electricity (Reverse Electrodialysis Heat Engine).

A preliminary analysis based on (i) activity coefficients, (ii) conductivity and (iii) solubility was performed in order to select the most suitable pure salt-water solutions for power production enhancement. This analysis resulted in the choice of LiCl, NH_4Cl and NaCl: LiCl was chosen for its really high activity coefficients and solubility, NH_4Cl for its high conductivity in water, while NaCl was used as reference salt. A preliminary analysis was carried out also for the choice of the salt binary mixtures by taking into account the same properties analysed for the pure salt cases. In particular, the multicomponent Pitzer model was used for assessing the salt activity coefficients in the mixture and the multicomponent Nernst equation was suitably modified for dealing with the salt binary mixtures to be investigated. On the basis of the results collected and also

for comparison purposes with the pure salt cases, mixtures composed of the above three salts (i.e. NaCl-LiCl, NH_4Cl-LiCl, NH_4Cl-NaCl) were identified as the most interesting. As concerns the pure salt-water solutions, results collected in a lab-scale RED stack equipped with Fujifilm® IEMs (optimized for NaCl) do not show a solution providing the highest corrected power density ($P_{D,corr}$) at any operating conditions. However, the use of NH_4Cl is suggested in the range of C_{high} investigated, while better performance in terms of power production are expected with the use of LiCl for larger C_{high}.

As regards the salt mixture experiments, the *OCV* values measured were always found included between the *OCVs* of the two corresponding pure salt solutions. Conversely, quite surprisingly, when C_{high} is equal to 0.5M and 5M, the R_{stack} measured for the salt binary mixtures was found lower than both the two values measured for the pure salts, thus resulting into a $P_{D,corr}$ being higher than both those relevant to the two pure salts.

This experimental evidence suggests that it could be possible to increase the power produced by a RED unit operating under typical conditions (as those investigated in the present work) and fed with NaCl-water solutions just by adding an equivalent molar quantity of another salt as LiCl or NH_4Cl.

Comparing the salt mixtures results collected, similar $P_{D,corr}$ were obtained for the three cases independently of C_{high}, although the NH_4Cl-LiCl mixture appears as the most promising.

On overall, the present work shows for the first time that RED stack performance in terms of power production can be enhanced by employing aqueous solutions of different salts. However, there is still large room for further investigations in order to understand better the complex interaction mechanism between ions, membrane fixed charges and water. This would allow guiding the choice of the salt combination features, in terms of salt type and quantity, to be used in a RED unit in order to maximize the electric power produced. Moreover, given the final aim to convert waste heat into power in a Reverse Electrodialysis Heat Engine, tests will also be needed to evaluate the performance of the regeneration unit fed by these salt mixture-water solutions.

ACKNOWLEDGEMENTS

REDstackBV is kindly acknowledged for providing us the RED unit used for the experiments and suggesting the use of salt mixtures to enhance performance.

FUJIFILM Manufacturing Europe® and DEUKUM® are kindly acknowledged for providing us the IEM membranes and the woven-spacers, respectively.
This work was performed within the RED-Heat-to-Power project (Conversion of Low Grade Heat to Power through closed loop Reverse Electro-Dialysis) - Horizon 2020 programme, Project Number: 640667: www.red-heat-to-power.eu.

NOMENCLATURE

A	membrane area [m^2]
A_ϕ, α, b	Pitzer model constant [$(kg/mol)^{1/2}$]
A_Λ, B_Λ, C_Λ	coefficients of Jones and Dole's equation
C	solution molarity [mol/l]
m	solution molality [mol/kg]
I	ionic strength [mol/kg]
Z	modified ionic strength [mol/kg]
f_γ	coefficient of Pitzer's model [-]
B_γ, C_γ	coefficients of Pitzer's model for pure salt-water solutions
B_{MX}, B'_{MX}, C_{MX}	coefficients of Pitzer's model for binary mixture-water solutions
ΔV	stack voltage [V]
I	stack current [A]
N	number of cell pairs [-]
P_D	Power Density [$W/(m^2N)$]
$P_{D,corr}$	Corrected Power Density [$W/(m^2N)$]
R	universal gas constant (8.314 J/(mol K))
R_{blank}	blank resistance [Ω]
R_{BL}	electrical resistance of the boundary layer [Ω]
R_{IEM}	electrical resistance of ionic exchange membrane [Ω]
R_{stack}	stack electrical resistance [Ω]
R_u	electrical resistance of the external load [Ω]
r	Jone and Dole's viscosity coefficient [$(l/mol)^{0.5}$]
s	Jone and Dole's viscosity coefficient [l/mol]
T	temperature [°C]
v	fluid velocity [cm/s]

z_M, z_X cation and anion charge [-]

Greek letters

α_p permselectivity [-]

η solution viscosity [Pa s]

γ_{MX} salt activity coefficient [-]

$\beta^{\square\square\square}$, $\beta^{\square\square\square}$, $\phi_{cc'}$, $\phi_{\square\square'}$ Pitzer model second order interaction parameters

$\psi_{Mca,}$ ψ_{Xca} Pitzer model third order interaction parameters

$\Delta\Phi_{cell}$ cell potential difference [V]

ν_M, ν_X cation and anion stoichiometric coefficients [-]

Λ_0 salt equivalent conductivity at infinite dilution [mS/(cm mol)]

Λ salt equivalent conductivity [mS/(cm mol)]

Subscripts

HIGH concentrate compartment

LOW dilute compartment

c, c' generic cation index

a, a' generic anion index

cell cell pair

Acronyms

AEM anion exchange membrane

CEM cation exchange membrane

IEM ion exchange membrane

OCV Open Circuit Voltage

PRO pressure retarded osmosis

RED reverse electrodialysis

SGP salinity gradient power

REFERENCES

[1] B.E. Logan, M. Elimelech, U. States, Membrane-based processes for sustainable power generation using water, Nature. 488 (2012) 313–319. doi:10.1038/nature11477.

[2] D.A. Vermaas, E. Guler, M. Saakes, K. Nijmeijer, Theoretical power density from salinity gradients using reverse electrodialysis, Energy Procedia. 20 (2012) 170–184. doi:10.1016/j.egypro.2012.03.018.

[3] J.W. Post, J. Veerman, H.V.M. Hamelers, G.J.W. Euverink, S.J. Metz, K. Nymeijer, C.J.N. Buisman, Salinity-gradient power: Evaluation of pressure-retarded osmosis and reverse electrodialysis, J. Memb. Sci. 288 (2007) 218–230. doi:10.1016/j.memsci.2006.11.018.

[4] S. Loeb, Large-scale power production by pressure-retarded osmosis, using river water and sea water passing through spiral modules, Desalination. 143 (2002) 115–122.

[5] A. Achilli, T.Y. Cath, A.E. Childress, Power generation with pressure retarded osmosis: An experimental and theoretical investigation, J. Memb. Sci. 343 (2009) 42–52. doi:10.1016/j.memsci.2009.07.006.

[6] F. Giacalone, A. Cipollina, F. Grisafi, A. Tamburini, G. Vella, G. Micale, Characterization of pressure retarded osmosis lab-scale systems, Desalin. Water Treat. 57 (2016) 22994–23006. doi:10.1080/19443994.2016.1173379.

[7] Strathmann, Ion-exchange membrane separation processes, 2004. doi:10.1017/CBO9781107415324.004.

[8] G.M. Geise, H.J. Cassady, D.R. Paul, B.E. Logan, M.A. Hickner, E. Logan, M.A. Hickner, Specific ion effects on membrane potential and the permselectivity of ion exchange membranes, Phys. Chem. Chem. Phys. 16 (2014) 21673–21681. doi:10.1039/C4CP03076A.

[9] P. Długołecki, K. Nymeijer, S. Metz, M. Wessling, Current status of ion exchange membranes for power generation from salinity gradients, J. Memb. Sci. 319 (2008) 214–222. doi:10.1016/j.memsci.2008.03.037.

[10] B. Zhang, J. Gi, S. Xie, S. Xia, Y. Chen, An integrative modeling and experimental study on the ionic resistance of ion-exchange membranes, J. Memb. Sci. 524 (2017) 362–369. doi:10.1016/j.memsci.2016.11.050.

[11] A. Daniilidis, D.A. Vermaas, R. Herber, K. Nijmeijer, Experimentally obtainable energy from mixing river water, seawater or brines with reverse electrodialysis, Renew. Energy. 64 (2014) 123–131. doi:10.1016/j.renene.2013.11.001.

[12] M. Tedesco, A. Cipollina, A. Tamburini, G. Micale, J. Helsen, M. Papapetrou, REAPower: use of desalination brine for power production through reverse electrodialysis, Desalin. Water Treat. 53 (2014) 3161–3169. doi:10.1080/19443994.2014.934102.

[13] M. Tedesco, A. Cipollina, A. Tamburini, I.D.L. Bogle, G. Micale, A simulation tool for analysis and design of reverse electrodialysis using concentrated brines, Chem. Eng. Res. Des. 93 (2015) 441–456. doi:10.1016/j.cherd.2014.05.009.

[14] A. Tamburini, M. Tedesco, A. Cipollina, G. Micale, M. Ciofalo, M. Papapetrou, W. Van Baak, A. Piacentino, Reverse electrodialysis heat engine for sustainable power production, Appl. Energy. (2017).

[15] A. Tamburini, A. Cipollina, M. Papapetrou, A. Piacentino, G. Micale, Salinity gradient engines, in: Sustain. Energy from Salin. Gradient, 2016: p. 219–256 (Chapter 7).

[16] A. Bevacqua, M., Tamburini, A., Papapetrou, M., Cipollina, A., Micale, G., Piacentino, Reverse electrodialysis with NH4HCO3-water systems for heat-to-power conversion, Energy. In Press (2017). doi:doi:10.1016/j.energy.2017.07.012.

[17] B. Ortega-Delgado, P. Palenzuela, D.-C. Alarcon-Padilla, Parametric study of a multi-effect distillation plant with thermal vapor compression for its integration into a Rankine cycle power block, Desalination. 394 (2016) 18–29. doi:10.1016/j.desal.2016.04.020.

[18] A. Cipollina, M.G. Di Sparti, A. Tamburini, G. Micale, Development of a Membrane Distillation module for solar energy seawater desalination, Chem. Eng. Res. Des. 90 (2012) 2101–2121. doi:10.1016/j.cherd.2012.05.021.

[19] X. Luo, X. Cao, Y. Mo, K. Xiao, X. Zhang, P. Liang, X. Huang, Power generation by coupling

reverse electrodialysis and ammonium bicarbonate : Implication for recovery of waste heat, Electrochem. Commun. 19 (2012) 25–28. doi:10.1016/j.elecom.2012.03.004.

[20] D. han Kim, B.H. Park, K. Kwon, L. Li, D. Kim, Modeling of power generation with thermolytic reverse electrodialysis for low-grade waste heat recovery, Appl. Energy. 189 (2017) 201–210. doi:10.1016/j.apenergy.2016.10.060.

[21] E. Fontananova, D. Messana, R.A. Tufa, I. Nicotera, V. Kosma, E. Curcio, W. Van Baak, E. Drioli, G. Di Pro, Effect of solution concentration and composition on the electrochemical properties of ion exchange membranes for energy conversion, J. Power Sources. 340 (2017) 282–293. doi:10.1016/j.jpowsour.2016.11.075.

[22] D.A. Vermaas, J. Veerman, M. Saakes, K. Nijmeijer, Influence of multivalent ions on renewable energy generation in reverse electrodialysis, Energy Environ. Sci. (2014) 1434–1445. doi:10.1039/c3ee43501f.

[23] A.H. Avci, P. Sarkar, R.A. Tufa, D. Messana, P. Argurio, E. Fontananova, G. Di, E. Curcio, Effect of Mg2+ ions on energy generation by Reverse Electrodialysis, J. Memb. Sci. 520 (2016) 499–506. doi:10.1016/j.memsci.2016.08.007.

[24] M. Bevacqua, A. Carubia, A. Cipollina, A. Tamburini, M. Tedesco, G. Micale, Performance of a RED system with ammonium hydrogen carbonate solutions, Desalin. Water Treat. 57 (2016) 23007–23018. doi:10.1080/19443994.2015.1126410.

[25] X. Zhu, W. He, B.E. Logan, Influence of solution concentration and salt types on the performance of reverse electrodialysis cells, J. Memb. Sci. 494 (2015) 154–160. doi:10.1016/j.memsci.2015.07.053.

[26] H.J. Cassady, E.C. Cimino, M. Kumar, M.A. Hickner, Specific ion effects on the permselectivity of sulfonated poly(ether sulfone) cation exchange membranes, J. Memb. Sci. 508 (2016) 146–152. doi:10.1016/j.memsci.2016.02.048.

[27] J.-H. Choi, H.-J. Lee, S.-H. Moon, Effects of Electrolytes on the Transport Phenomena in a Cation-Exchange Membrane., J. Colloid Interface Sci. 238 (2001) 188–195. doi:10.1006/jcis.2001.7510.

[28] M.C. Martí-Calatayud, D.C. Buzzi, M. García-Gabaldón, A.M. Bernardes, J.A.S. Tenório, V. Pérez-Herranz, Ion transport through homogeneous and heterogeneous ion-exchange membranes in single salt and multicomponent electrolyte solutions, J. Memb. Sci. 466 (2014) 45–57. doi:10.1016/j.memsci.2014.04.033.

[29] L. Dammak, R. Lteif, G. Bulvestre, G. Pourcelly, B. Auclair, Determination of the diffusion coefficients of ions in cation-exchange membranes, supposed to be homogeneous, from the electrical membrane conductivity and the equilibrium quantity of absorbed electrolyte, Electrochim. Acta. 47 (2001) 451–457. doi:10.1016/S0013-4686(01)00743-5.

[30] M. Tedesco, C. Scalici, D. Vaccari, A. Cipollina, A. Tamburini, G. Micale, Performance of the first reverse electrodialysis pilot plant for power production from saline waters and concentrated brines, J. Memb. Sci. 500 (2016) 33–45. doi:10.1016/j.memsci.2015.10.057.

[31] M. Tedesco, A. Cipollina, A. Tamburini, G. Micale, Towards 1 kW power production in a reverse electrodialysis pilot plant with saline waters and concentrated brines, J. Memb. Sci. 522 (2017) 226–236. doi:10.1016/j.memsci.2016.09.015.

[32] A. Salis, B.W. Ninham, Models and mechanisms of Hofmeister effects in electrolyte solutions, and colloid and protein systems revisited, Chem. Soc. Rev. 43 (2014) 7358–7377. doi:10.1039/C4CS00144C.

[33] R. Zangi, Can Salting-In / Salting-Out Ions be Classified as Chaotropes / Kosmotropes ?, J.Phys.Chem.B. 114 (2010) 643–650.

[34] B. Hribar, N.T. Southall, V. Vlachy, K.A. Dill, How Ions Affect the Structure of Water, JACS Artic. (2002) 12302–12311.

[35] K.S. Pitzer, Thermodynamics of Electrolytes. I. Theoretical Basis and General Equations, J. Phys. Chem. 77 (1973) 268–277. doi:10.1021/j100621a026.

[36] N. Lakshminarayanaiah, Transport phenomena in artificial membranes, Chem. Rev. 65 (1965)

491–565. doi:10.1021/cr60237a001.

[37] G. Jones, C.F. Bickford, The Conductance of Aqueous Solutions as a Function of the Concentration. I. Potassium Bromide and Lanthanum Chloride, J. Am. Chem. Soc. 56 (1934) 602–611.

[38] D.W. Green, R.H. Perry, Perry's Chemical Engineers' Handbook, 2008.

[39] V.M.M.Q. Lobo, Handbook of electrolyte solutions, 1989.

[40] E. Shaulsky, C. Boo, S. Lin, M. Elimelech, Membrane-Based Osmotic Heat Engine with Organic Solvent for Enhanced Power Generation from Low-Grade Heat, Environ. Sci. Technol. 49 (2015) 5820–5827. doi:10.1021/es506347j.

[41] K.S. Pitzer, J.J. Kim, Thermodynamics of Electrolytes. IV. Activity and Osmotic Coefficients for Mixed Electrolytes, J. Am. Chem. Soc. 96 (1974) 5701–5707. doi:10.1021/ja00825a004.

[42] R.P. Buck, Interfacial potential differences at mixed conductor interfaces: Nemst Distribution and generalizations, J. Electroanal. Chem. 292 (1990) 73–91.

[43] P. Vanýsek, R.P. Buck, Multi-ion Nernst distribution potential equations: interfacial potentials at equilibrium liquid/liquid and membrane interfaces, J. Electroanal. Chem. 297 (1991) 19–35. doi:10.1016/0022-0728(91)85356-T.

[44] O. Scialdone, C. Guarisco, S. Grispo, A.D. Angelo, A. Galia, Investigation of electrode material – Redox couple systems for reverse electrodialysis processes. Part I: Iron redox couples, J. Electroanal. Chem. 681 (2012) 66–75. doi:10.1016/j.jelechem.2012.05.017.

[45] E. Güler, W. van Baak, M. Saakes, K. Nijmeijer, Monovalent-ion-selective membranes for reverse electrodialysis, J. Memb. Sci. 455 (2014) 254–270. doi:10.1016/j.memsci.2013.12.054.

[46] L. Gurreri, A. Tamburini, A. Cipollina, G. Micale, M. Ciofalo, CFD prediction of concentration polarization phenomena in spacer- filled channels for reverse electrodialysis, J. Memb. Sci. 468 (2014) 133–148. doi:10.1016/j.memsci.2014.05.058.

[47] L. Gurreri, A. Tamburini, A. Cipollina, G. Micale, M. Ciofalo, Flow and mass transfer in spacer-filled channels for reverse electrodialysis: a CFD parametrical study, J. Memb. Sci. 497 (2016) 300–317. doi:10.1016/j.memsci.2015.09.006.

[48] S. Pawlowski, P. Sistat, J.G. Crespo, S. Velizarov, Mass transfer in reverse electrodialysis: Flow entrance effects and diffusion boundary layer thickness, J. Memb. Sci. 471 (2014) 72–83. doi:10.1016/j.memsci.2014.07.075.

[49] A.H. Galama, D.A. Vermaas, J. Veerman, M. Saakes, H.H.M. Rijnaarts, J.W. Post, K. Nijmeijer, Membrane resistance: The effect of salinity gradients over a cation exchange membrane, J. Memb. Sci. 467 (2014) 279–291. doi:10.1016/j.memsci.2014.05.046.

[50] N.P. Berezina, N.A. Kononenko, O.A. Dyomina, N.P. Gnusin, Characterization of ion-exchange membrane materials: Properties vs structure, Adv. Colloid Interface Sci. 139 (2008) 3–28. doi:10.1016/j.cis.2008.01.002.

[51] M. Geise, A.J. Curtis, M.C. Hatzell, M.A. Hickner, B.E. Logan, Salt Concentration Differences Alter Membrane Resistance in Reverse Electrodialysis Stacks, (2014) 8–11.

[52] A.H. Galama, Ion exchange membranes in seawater applications. Processes and characteristics, 2015.

[53] G.M. Geise, D.R. Paul, B.D. Freeman, Fundamental water and salt transport properties of polymeric materials, Prog. Polym. Sci. 39 (2014) 1–24. doi:10.1016/j.progpolymsci.2013.07.001.

APPENDIX A

Table A1: Parameters relevant to the calculation of the activity coefficient and the equivalent conductivity of pure salt-water solutions.

Pure salt solution parameters				
		NaCl	NH_4Cl	LiCl
Activity coefficients parameters	$\beta^{(0)}$	0.0765	0.0522	0.1494
	$\beta^{(1)}$	0.2664	0.1918	0.3074
	C^{Φ}	0.00127	-0.00301	0.00359
Equivalent conductivity parameters	λ_0	126.5	149.6	114.97
	A_Λ	91.0239	149.6	42.975
	B_Λ	1.6591	3.4498	0.1045
	C_Λ	6.8041	4.3620	0.00735

Table A2: Parameters relevant to the calculation of the activity coefficients of salts in salt binary mixture-water solutions.

Salt mixture parameters for activity coefficient calculation					
Common parameters		Specific mixture parameters			
A_Φ $[(kg/mol)^{1/2}]$	0.3915		NaCl-NH_4Cl	NH_4Cl-LiCl	LiCl-NaCl
b $[(kg/mol)^{1/2}]$	1.2	$\Phi_{cat\text{-}cat}$	0.0044	-0.0563	0.012
α $[(kg/mol)^{1/2}]$	2	$\Psi_{cat\text{-}cat\text{-}an}$	-0.0031	0.0089	-0.003